Petrology and Geochemical Constraints on the Origin of Banded Iron Formation-Hosted Iron Mineralization from the Paleoproterozoic Nyong Serie (Congo Craton, South Cameroon), Pout Njouma Area (Edea North): Evidence for Iron Ore Deposits

Ndema Mbongué Jean-Lavenir[1,2], Aroke Eric Alemnju [1]

[1]*Department of Geology, University of Buea; Buea, Cameroon*

[2]*Laboratory of Petrology and Structural Geology, Department of Earth Science, UY I; Yaoundé, Cameroon*

Abstract: **The Pout Njouma area is located in the Nyong unit, which is the northwestern extension of the Congo Craton in southern Cameroon. The assessment of iron mineralization in this area is carried out through rock sampling survey. Representative rock samples were analysed by inductively coupled plasma mass spectrometry (ICP-MS) combined with instrumental neutron activation analysis (INAA) technologies to completely characterize the iron- rich rock samples. The Pout Njouma area is made up of magnetite- gneiss, magnetite-quartzite and banded iron formations; these rocks display microband textures and granoblastic microstructures. The mineral assemblages indicate that magnetite- gneiss and magnetite- quartzite have been metamorphosed under greenschist facies conditions, while banded iron formations display the paragenesis of greenschist to amphibolite facies. This iron deposit belongs to the oxide facies, with magnetite and quartz being the common predominant minerals while sericite and limonite occur as accessory minerals. The Pout Njouma iron occurrence exhibits significant concentration of Fe_2O_3 + SiO_2 (95%), relative elevated values of Al_2O_3 and TiO_2 contents, lower high field strength elements (Y, Hf, Sc, Zr) and variation in enrichment in transition metals. Post Archaean Australian Shale- normalized rare earth elements patterns show slight enrichment in light rare earth elements relative to heavy rare earth elements. The Pout Njouma iron deposits have the composition of Fe-sand, and their geochemical signature indicates that low input of detrital materials contributed to the chemical precipitation of their formation. The absence of a large positive Eu anomaly (Eu/Eu* = 1.01-1.54) indicates that an important role of low-temperature hydrothermal solutions contributed to the deposition of the Pout Njouma ion deposits. Pout Njouma area is of low grade siliceous ore (43.19 to 48.49% Fe_2O_3) corresponding to depleted iron ore (30 to 50% Fe). The Pout Njouma iron deposits derived from Precambrian rocks which were deposited in an oceanic island-arc margin (ARC) setting where conditions were anoxic and fast sedimentation. The average chemical composition of Pout Njouma iron formations is compared with the known BIFs and the result show SiO_2 and Fe_2O_3 enrichment except in Mballam and Mayo Binka where Fe shows significant elevated values compared with SiO_2. Also, data show low concentration of Al_2O_3, TiO_2, CaO and MnO, which infers the non-volcanogenic origin.**

***Keywords*: Pout Njouma area, Nyong unit, low-temperature hydrothermal solutions, low grade siliceous ore, Precambrian**

I. INTRODUCTION

Banded iron formations (BIFs) consist of chert (silica) interlayered with iron oxide, iron carbonate, or iron silicate minerals, and occur nearly exclusively in marine sedimentary strata of Precambrian age [1]. Though they now occur on land, they are generally known to have originated in marine environment. Lack of terrestrial detritus in the marine finely bedded BIF suggested low-energy settings, far from the coast and the occurrence of BIFs in huge basins in several countries was referred to deposition in the oceans [2]. Iron formations were deposited for more than three billion years, but as the Earth system changed fundamentally, so too did the style of iron-formation deposition. The formations are abundant around the time of the great oxygenation event (GOE), 2400 Ma, and become less common after 1800 Ma with evidence pointing to intermittent low levels of free atmospheric oxygen [3]. Major BIF deposition ended at ca. 1.8 Ga [1]. Aspects of, and changes in, the Earth system that are most relevant to the deposition of iron formation include volcanism, evolution of the biosphere, and ocean composition [4], [5]. Different explanations have been offered for this global termination of iron mineralization, including changes in the redox state of the deep ocean from anoxic to oxic or anoxic to sulphuric [5], the deepening of mid-ocean ridges and decreased heat flow after 1.8 Ga [6], and also as a result of the oceanic impact of the giant Sudbury extra-terrestrial bolide [7]. In all of these models, the end of BIFs deposition at ca. 1.8 Ga is attributed, explicitly or implicitly, to gradual processes in the evolution of the lithosphere, hydrosphere, or atmosphere during the Earth's history.

Banded iron formation is an interesting rock type because of the absence of a modern analogue and of its economic importance. It is significant for understanding the geologic processes operating during the early history of the Earth.

According to [8], iron-formations are chemical sediments, typically thin-bedded or laminated, containing 15% or more iron of sedimentary origin, commonly but not necessarily containing layers of chert. The iron-minerals are commonly interlayered with quartz, chert and carbonates [9]. Four different mineral facies can be found in BIFs: oxide, silicate, carbonate and sulphide [3], [8]-[11]. The sulphide facies is pyritic carbonaceous shale or slate and not really a type of iron-formation even though it is a constituent of some BIFs [12], [13]. The oxide facies consists predominantly of magnetite or hematite interlayered with silica, carbonates, iron silicates or some combination of these minerals [14]. The carbonate facies is characterized by the presence of siderite and reflects strongly reducing condition with a $P_{CO2} \geq 10^{-3.5}$ atm [15]. Associated carbonate minerals are ankerite, dolomite, and calcite. The silicate facies is characterized by iron-rich silicate minerals.

Texturally [13] and according to the scale of banding, BIFs are microbanding (millimeter to submillimeter) to macroband (meter in thickness) via mesobands (centimeter-thick units). Trendall and Blockley (1970) introduced the terms mesobanding for such bands in the course of a detailed description of the BIFs, and microbanding for a regular small-scale lamination within many, but not all chert mesobands. Microbands are defined by a concentration of some Fe minerals (either hematite, magnetite, carbonate, stipnomelane or some combination of these) within the pervasive silica framework, a single microband being defined by an iron- rich component in which they are effectively absent. BIF macroband [17] is characterized by silica- rich (iron- poor) mesobands of chert alternating with iron- rich (silica- poor) mesobands, to which [16] applied the name chert matrix.

There are four different types of iron formations based on lithology, composition, associated rocks and their depositional environment: (i) Clinton type and Minette type consist of grained iron formations (GIFs); they have a granular texture with the absence of laminations/banding; (ii) Algoma- type and Superior- type called banded iron formations (BIFs) are mainly banded cherty rocks and provide the major part of the world iron production [10]. The principal difference between Algoma- type and Superior- type is the depositional environment. Basically, Algoma- type iron formations have a small extension and have been deposited as chemical sediments along with other sedimentary rocks and volcanic in and adjacent to volcanic arcs and spreading centres; whereas Superior- type iron formations have a large lateral extension, and were chemically precipitated on marine continental shelves and in shallow basins [3], [9]-[14]. Algoma- and Superior- type contain similar mineralogy [3]. However, stilpnomelane is a mineral only present in Algoma- type [18]. It usually reflects contamination with volcaniclastic detritus [19], [20]. The four different facies that can be found in BIFs (oxide, silicate, carbonate and sulphide facies) reflect their depth of formation, Eh/pH conditions that resulted due of variations in composition of the seawater in the sedimentary basin and subsequently reflect the type of BIF that occurs [3], [8]-[11].

The rapid economic growth in certain countries like India and China has led to an increase in the demand for steel in the world market. As such there has been an increase in Fe ore exploration to meet up with this demand. Giant hematite and martite-goethite iron ores (≥ 56% Fe) derived from iron formations rank among the largest ore deposits and are the principal source of iron for the global steel industry. Given their economic importance, iron formations have been extensively studied, during the past one hundred years, but many aspects of their sedimentary origin remain enigmatic because modern analogues are unknown [3]. In Cameroon, the Archaean greenstone belt crops in the southern part of the country within the Ntem complex which corresponds to the northern edge of the Congo Craton. The BIF occurrence within this Precambrian Ntem Complex in southern Cameroon have been widely reported [21]-[36]. Despite of all of these works, published data on the BIF occurrence in Cameroon in general and in Edea North in particular are still largely lacking. The aim of this work is to present a detailed geologic and geochemical study of the Pout Njouma iron occurrence and investigate for the origin of iron ore mineralizations.

II. Geologic Setting

The Pout Njouma area (situated in Edea North) is located within the Ntem Complex which is the northwestern margin of the Archaean Congo Craton, bordered in the north by the Yaoundé Group [37] of the Pan-African orogenic belt in Central Africa (Fig. 1a, 1b). The Ntem Complex contains the oldest geological formations in Cameroon predominantly made up of Archaean rocks that were partially reworked during the Palaeoproterozoic–Transamazonian and Pan-African–Braziliano cycles [38]-[42]. This Precambrian basement of southern Cameroon experienced a thermotectonic evolution which favoured the emplacement of ferriferous formations commonly called band iron formations (BIFs) or itabirites, with the BIFs being the subcrustal formations which form the greenstone belt [43]. The Ntem BIFs basically consist of oxide-facies and silicate-facies BIF, which are spatially associated with different wallrock types such as gneiss, quartzite, schist, amphibolite, syenite, and rarely epidotite–serpentinite [21], [24], [29], [30]; [32]-[34]. The majority of the Ntem BIFs have undergone a greenschist to granulite facies metamorphic grade, where significant banded iron formations (BIFs)-hosted iron deposits have been discovered [29], [32]. The Ntem complex is subdivided into three units: the Ayna unit, the Ntem unit and the Nyong unit respectively from the East to the West.

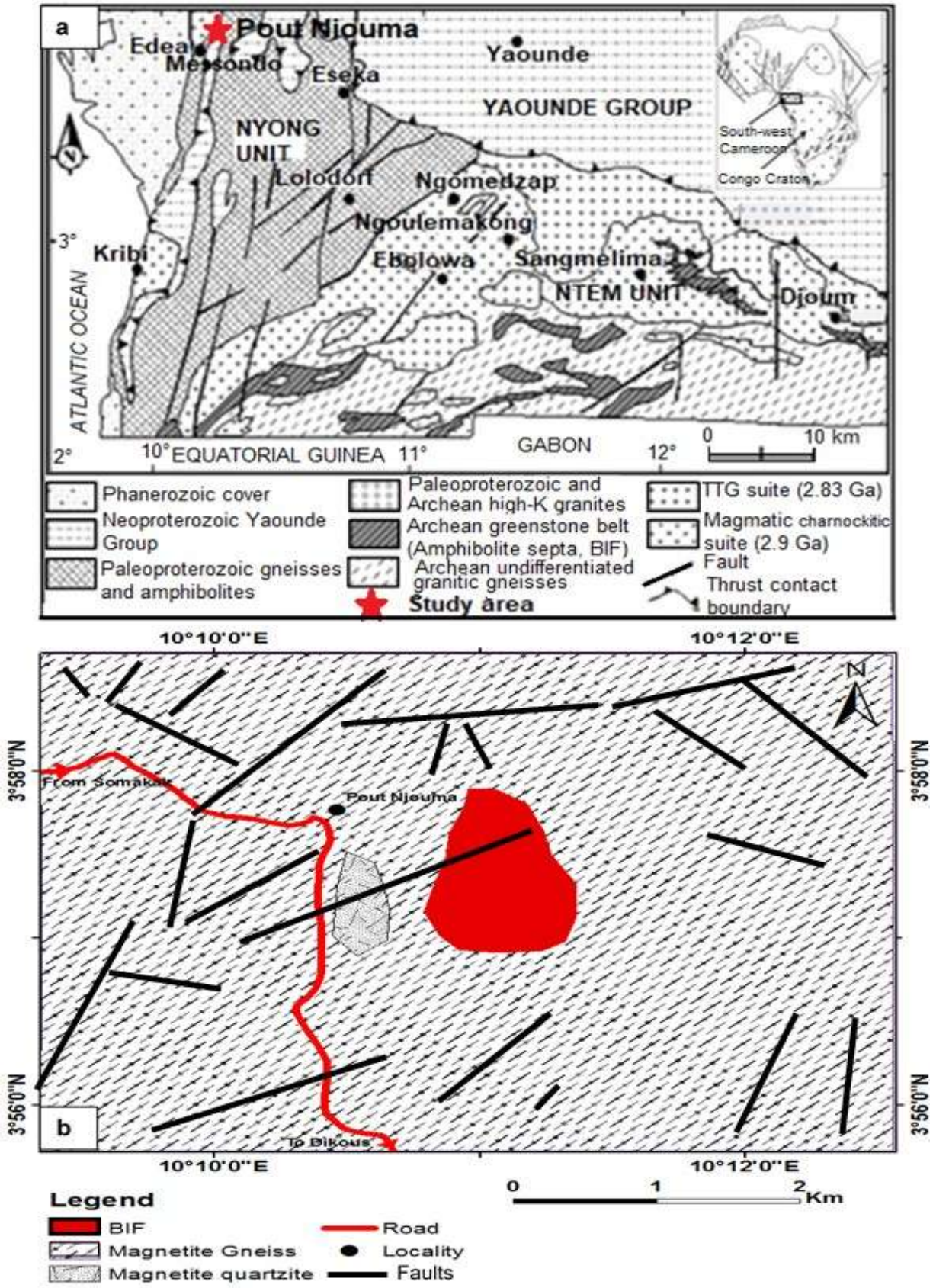

Fig. 1. (a) Geologic map of South-West Cameroon as modified from [44] showing the lithologic units of Congo Craton in Cameroon and the studied area, (b) detailed geologic map of Pout Njouma area.

The Ayna unit is still unknown, meanwhile some studies revealed in this unit the presence of migmatites, greenstones and intrusive granitoids. The Ayna unit is Paleoproterozoic in age and the Rb/Sr and K/Ar of two intrusive granodiorites have been dated at 1866 ± 55 Ma and 2027 ± 101 Ma respectively [44]. The Ntem unit is dominated by plutonic rocks of the charnockite suite and by intrusive tonalites, trondhjemites and granodiorites (TTG), dated at 2.9 Ga [38], [45], [46]. The Pout Njouma area (Fig. 1b) is found within the Nyong unit. The Nyong unit, located in the NW corner of the Congo craton constitutes the main Paleoproterozoic unit in Cameroon and is a well-preserved granulitic unit of the West Central African Belt resting as an Eburnean nappe on the Congo Craton [38], [46], [47]. The works of [41] and [48] reveal that the Nyong unit consists of metasedimentary and metavolcanic rocks, syn-to late-tectonic granitoids and syenites. The other lithologies encountered in the Nyong unit include: metamorphosed mafic–ultramafic rocks, expressed as pyroxenites and amphibolites [49], orthogneisses and metaquartzites with a dominance of biotite-amphibole-gneiss, pyrigarnite and magnetite-bearing gneiss [23]. The main plutonic rocks include syn- to late-tectonic charnockites, alkaline syenites and post-tectonic metadiorites [38], [47].

III. Methods of Investigation

Systematic scouting of the study area in search of outcrops and mapping was accomplished with the help of a field guide. Samples were collected from several discontinuous outcrops in the Pout Njouma area and proper care was taken to collect best possible fresh sample. At each sample point, outcrops were described, global positioning system (GPS) coordinates registered, photographs taken and representative samples collected. In total, 12 samples were collected from the study area. The registered GPS readings were subsequently used to come out with a geologic map of the study area.

Six representative rock samples were sent to the Institute of Geological Research and Mining (IGRM) Laboratory in Yaoundé (Nkolbisong) for the preparation of thin sections. The rocks were cut using a rock cutter in to rectangular cubes (4×2.5×1 cm) and placed on a glass slide using araldite gum. It is then polished until a thin section of 0.3 mm is reached. Microstructure and mineralogical studies were done using a petrographic microscope in the Geology Laboratory at the Department of Geology in the University of Buea.

Whole rock geochemical analysis was realized on six samples of iron rich rock. Samples were submitted to Activation Laboratories (ACTLABS) in Canada for geochemical analysis following Total IDENT/4E-expl, analytic code 4E [50]. This package uses inductively coupled plasma (ICP) and instrumental neutron activation analysis (INAA) technologies to completely characterize geological samples. A minimum sample weight of 5g is required. The major elements were analyzed by fusion-inductively coupled plasma (FUS-ICP) and they are expressed in percentage (%) of major oxides, with the detection limits varying from 0.005 to 0.01%. Loss of ignition (LOI) was determined by gravimetry (GRAV). Trace elements are analyzed by multiple techniques combining ICP and INAA analytical techniques. They are expressed in part per million (ppm), with the detection limits ranging from 0.1 to 20 ppm. Rare earth elements are expressed in ppm. They were analyzed by instrumental neutron activation analysis (INAA) methods with the detection limits ranging from 0.05 to 5 ppm.

IV. Results

A. Petrography

The Pout Njouma area is made up of magnetite- gneiss, magnetite- quartzite and banded iron formations (Fig. 1b). Mineral abbreviations recommendations by the IUGS Subcommission on the Systematics of Metamorphic Rocks are according to [51].

1) Magnetite- Gneiss

Magnetite- gneisses outcrop as boulders as a dark grey rock displaying medium grained (Fig. 2a). This rock type is weakly foliated characterized by alternation of quartz + feldspar-rich millimetric light bands and fine ferromagnesian-rich dark bands. They have a moderate to strong attraction with the magnetic pen. In thin section, magnetite- gneisses show a granoblastic microstructure (Fig. 2b) made up of quartz (25-30%), orientated magnetite (15-20%), subhedral plagioclase crystals (20-25%) and anhedral biotite minerals (15-20%). The metamorphic assemblage recorded in the magnetite-gneisses and that characterizes the greenschist facies is Qtz + Mgt + Pl +Bt.

2) Magnetite- Quartzite

Magnetite-quartzite outcrops as blocks and boulders. The representative rock samples are light grey in colour (Fig. 2c), medium grained and moderately magnetic. Under the microscope, they display a granoblastic microstructure (Fig. 2d) made up of quartz (40-50%), biotite (15-20%), magnetite (20-25%), plagioclase (≈ 2%), and limonite (≈ 1%) as accessory mineral. Magnetite-quartzite shows also a paragenesis of greenschist facies characterized by the mineral assemblage of Qtz + Mgt + Pl + Bt ± Lm.

3) Banded Iron Formations

The banded iron formation (BIFs) from Pout Njouma area are characterized by irregular thickness and discontinuous alternating white quartz- rich and dark iron oxide layers (Fig. 2e). The rock is strongly magnetic and occurs as small blocks (10 to 50 cm), most of which are highly weathered. The rock has a microband texture characterized by millimeter to submillimeter regular small-scale lamination within many silica mesobands. Under the microscope, the BIF is generally characterized by intercalated quartz- rich grey-white and magnetite- rich dark bands (Fig. 2f), and they exhibit granoblastic microstructure (Fig. 7f, 2g). They are made of ribbons of quartz (25-35%) that define the silica- rich layers (Fig. 7f, 2g), euhedral and subhedral-shaped magnetite crystals (25-30%), plagioclase (≈ 5%), hornblende (10-20%), and disseminated limonite (≈ 3%) and sericite (≈ 2%) as accessory phase. This iron formation shows the parageneses ranging between greenschist facies (Mgt + Qtz ± Pl + Ser ± Lm) to amphibolite facies (Mgt + Qtz ± Pl + Hbl ± Ser ± Lm).

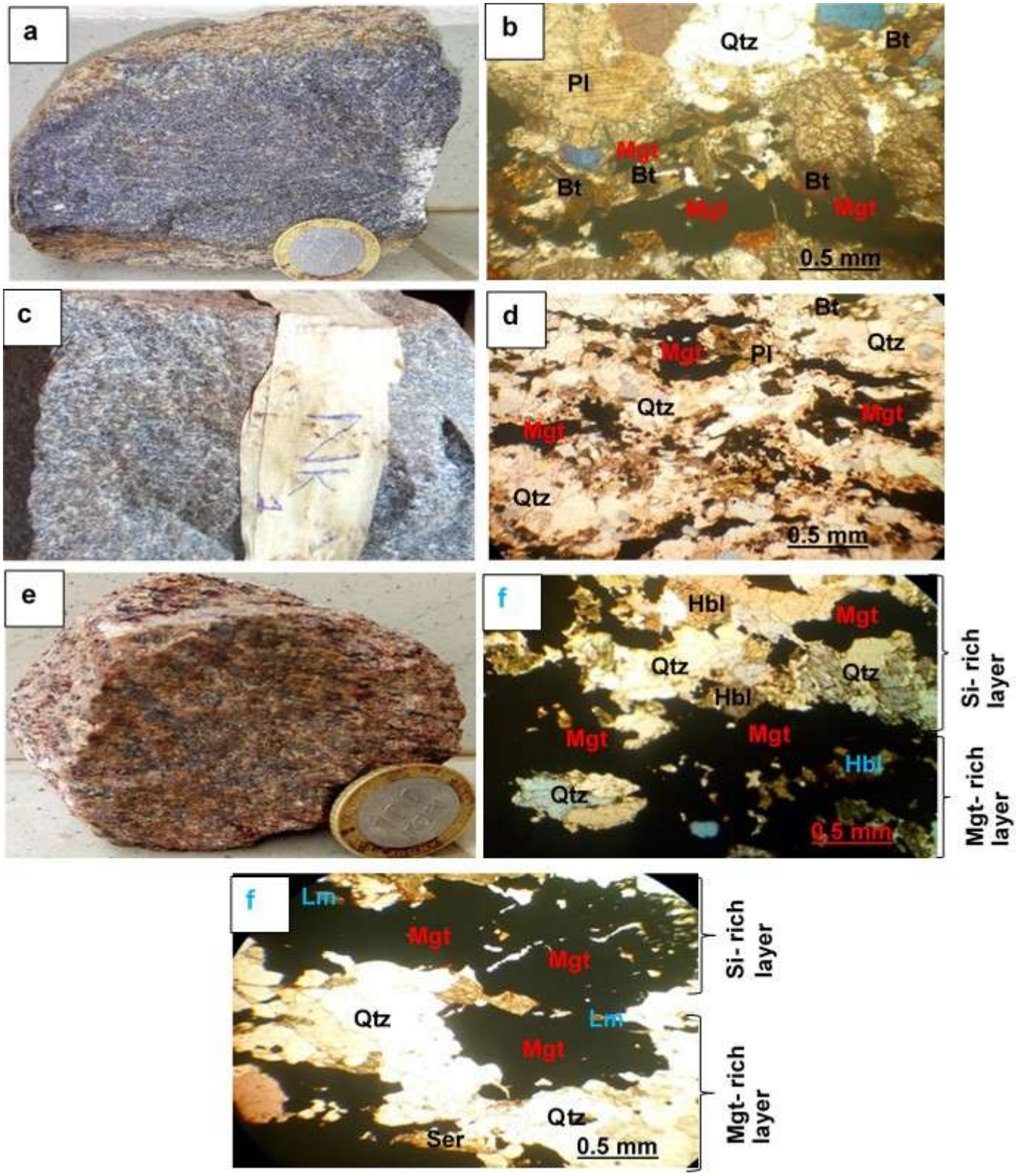

Fig. 2. Macro- and microphotographs of Pout Njouma iron occurrence. (a, b): magnetite-gneiss, (c, d): magnetite-quartzite and (e, f, h): BIFs.

B. Whole-Rock Geochemistry

Whole-rock geochemical analysis was realized on six (06) representative samples of iron formations in term of major Elements, trace elements and rare earth elements, and the analytic data are presented in Table 1.

TABLE I

CHEMICAL COMPOSITION OF POUT NJOUMA IRON FORMATIONS

Analyte Symbol	Detection Limit	Analysis Method	Samples					
			PD3	PD6	PD12	PD13	PD14	PD15
SiO_2 (%)	0.01	FUS-ICP	50.46	53.32	46.02	49.82	46.61	52.17
TiO_2	0.005	FUS-ICP	0.386	0.087	0.537	0.86	0.394	0.322
Al_2O_3	0.01	FUS-ICP	1.81	1.05	2.04	2.81	2.08	2.68
Fe_2O_3(T)	0.01	FUS-ICP	45.13	45.85	48.49	44.14	47.83	43.19
MgO	0.01	FUS-ICP	1.8	0.75	1.65	1.96	2.06	1.28
MnO	0.01	FUS-ICP	0.08	0.05	0.12	0.13	0.1	0.09
CaO	0.01	FUS-ICP	0.3	0.05	0.33	0.74	0.4	0.52
Na_2O	0.01	FUS-ICP	0.04	0.01	0.03	0.15	0.25	0.11
K_2O	0.01	FUS-ICP	0.03	< 0.01	0.03	0.24	0.05	0.47
P_2O_5	0.01	FUS-ICP	0.1	0.09	0.19	0.26	0.14	0.08
SO_3	0.001	TD-ICP	0.007	0.006	0.004	0.027	0.011	0.015
LOI		GRAV	0.49	-0.51	-0.61	-0.59	-0.9	-0.35
Total	0.01	FUS-ICP	100.6	100.8	98.81	100.5	99.01	100.6
Ag (ppm)	0.5	MULT INAA / TD-ICP	< 0.5	< 0.5	< 0.5	< 0.5	< 0.5	< 0.5
As	2	INAA	< 2	< 2	< 2	< 2	< 2	< 2
Au (ppb)	5	INAA	< 5	< 5	< 5	< 5	< 5	< 5
Ba	3	MULT INAA/FUSICP	33	38	45	520	140	499
Be	1	FUS-ICP	< 1	< 1	< 1	< 1	< 1	< 1
Bi	2	TD-ICP	5	5	5	6	7	5
Br	1	INAA	< 1	< 1	< 1	< 1	< 1	< 1
Cd	0.5	TD-ICP	1.2	1.2	1.4	1.1	1.3	1.1
Co	1	INAA	15	6	16	17	15	10
Cr	1	INAA	17	16	19	17	19	26
Cs	0.5	INAA	< 0.5	< 0.5	< 0.5	< 0.5	< 0.5	< 0.5
Cu	1	TD-ICP	9	7	6	20	9	8
Hf	0.5	INAA	< 0.5	< 0.5	< 0.5	< 0.5	0.7	0.8
Hg	1	INAA	< 1	< 1	< 1	< 1	< 1	< 1
Ir	5	INAA	< 5	< 5	< 5	< 5	< 5	< 5
Mo	2	TD-ICP	< 2	< 2	< 2	< 2	< 2	< 2
Ni	1	TD-ICP	58	18	37	35	40	26
Pb	5	TD-ICP	8	11	12	< 5	< 5	7
Rb	20	INAA	< 20	20	< 20	< 20	< 20	30
Sb	0.2	INAA	< 0.2	< 0.2	< 0.2	< 0.2	< 0.2	< 0.2
Sc	0.1	INAA	4.7	2.1	9.4	11.6	6.6	6.8

TABLE II : CONTINUED

Se	3	INAA	< 3	< 3	< 3	< 3	< 3	< 3
Sr	2	FUS-ICP	3	6	6	21	9	30
Ta	1	INAA	< 1	< 1	< 1	< 1	< 1	< 1
Th	0.5	INAA	< 0.5	0.9	0.6	2	1.8	< 0.5
U	0.5	INAA	< 0.5	< 0.5	< 0.5	< 0.5	< 0.5	< 0.5
V	5	FUS-ICP	63	7	64	132	43	38
W	3	INAA	< 3	< 3	< 3	< 3	< 3	< 3
Y	1	FUS-ICP	5	< 1	7	19	8	18
Zn	1	TD-ICP	45	16	103	80	73	60
Zr	2	FUS-ICP	18	15	5	23	36	30
La	0.2	INAA	26.6	35	21	36	13.3	26.7
Ce	3	INAA	32	46	17	32	15	33
Nd	5	INAA	25	24	15	40	11	23
Sm	0.1	INAA	5	3.5	3.5	8.5	2.7	6.6
Eu	0.1	INAA	1.2	0.7	0.7	1.8	0.9	1.6
Tb	0.5	INAA	< 0.5	< 0.5	< 0.5	1	< 0.5	< 0.5
Yb	0.1	INAA	1.1	0.3	1	1.9	1.1	2.2
Lu	0.05	INAA	0.13	< 0.05	0.13	0.23	0.13	0.28
ΣREE			91.53	110.05	58.83	121.43	44.65	93.88
$(La/Yb)_N$			1.78	8,60	1.55	1.40	0.89	0.894
$(Tb/Yb)_N$			1.65	6.06	1.82	1.91	1.65	0.83
Eu/Eu*			1.34	1.005	1.005	1.13	1.52	1.45
Ce/Ce*			0.42	0.52	0.20	0.46	0.19	0.42
Mass (g)		INAA	2.076	2.104	2.248	2.033	2.299	1.96

1) Major Elements

Major elements data of the representative samples of Pout Njouma iron prospect are reported in Table 1. The bulk chemical composition of the analyzed rock samples shows SiO_2 and Fe_2O_{3T} values range from 46.02 to 53.32 wt. % (average: 49.73 wt. %) and 43.19 to 48.49 wt. % (average: 45.77 wt %) respectively, which suggests that SiO_2 and Fe_2O_3 are the dominant components. These two major oxides are the most important components in the Pout Njouma iron deposit and they represent 95.05% of the bulk rock composition while the other major elements represent 4.95 %. There is a strong negative correlation between Fe_2O_{3T} and SiO_2 (r = -0.76, Table 2; Fig. 3) suggesting the incorporation of Fe_2O_3 and SiO_2 in different mineral phases. Also Fe_2O_{3T} shows negative correlation with K_2O (r = -0.76) and SO_3 (r = - 0.61; Table 2; Fig. 3). The presence of Al_2O_3 (1.05 to 2.81%) and TiO_2 (0.087 - 0.86%) suggest trace inputs of detrital material. Al_2O_3 shows a strong positive correlation with TiO_2 (r = 0.74; Table 2) and a very strong positive correlation with CaO (r = 0.96; Table 2). MgO (0.75 to 2.06 wt. %) and CaO (0.05 - 0.74) contents are very low. The low contents of these two elements combined with the low LOI (0.9 - 0.49%) indicate lack of carbonate and silicate minerals. Pout Njouma iron rock samples exhibit a composition of poor- alkali rocks with a total alkali content ($Na_2O + K_2O$) ranges between 0.025 to 0.58% reflecting the rarity of silicate minerals. The other major oxides occur in low percentages and a very strong positive correlation is observed between TiO_2 and MnO (r = 0.93), TiO_2 and P_2O_5 (r = 0.92), while CaO (r = 0.84) and Al_2O_3 (r = 0.74) display strong positive correlation with TiO_2 (Table 2).

TABLE III

Pearson's correlation matrix for Pout Njouma iron prospect

	SiO_2	Al_2O_3	Fe_2O_3	MnO	MgO	CaO	Na_2O	K_2O	TiO_2	P_2O_5	SO_3	Nd	V	Cr	Rb	Sr	Y	Zr	Ba	Hf	Ni	Zn	Pb	Sc	Co	Th
SiO_2	1.00																									
Al_2O_3	-0.23	1.00																								
Fe_2O_3	-0.76	-0.42	1.00																							
MnO	-0.68	0.78	0.13	1.00																						
MgO	-0.73	0.57	0.22	0.75	1.00																					
CaO	-0.22	0.97	-0.43	0.81	0.63	1.00																				
Na_2O	-0.40	0.53	0.05	0.43	0.64	0.57	1.00																			
K_2O	0.35	0.75	-0.76	0.23	-0.06	0.65	0.25	1.00																		
TiO_2	-0.47	0.75	-0.08	0.93	0.73	0.84	0.35	0.21	1.00																	
P_2O_5	-0.51	0.50	0.16	0.85	0.58	0.64	0.28	-0.04	0.92	1.00																
SO_3	0.13	0.76	-0.61	0.53	0.37	0.88	0.52	0.62	0.70	0.58	1.00															
Nd	0.50	0.35	-0.73	0.18	-0.01	0.50	-0.13	0.36	0.50	0.43	0.74	1.00														
V	-0.32	0.70	-0.21	0.83	0.69	0.82	0.27	0.20	0.98	0.87	0.73	0.64	1.00													
Cr	0.08	0.55	-0.37	0.11	-0.09	0.34	0.22	0.82	-0.11	-0.34	0.12	-0.23	-0.19	1.00												
Rb	0.40	0.46	-0.61	-0.09	-0.30	0.28	0.06	0.89	-0.21	-0.44	0.19	0.00	-0.23	0.94	1.00											
Sr	0.30	0.77	-0.71	0.30	-0.03	0.71	0.35	0.98	0.28	0.09	0.71	0.40	0.26	0.75	0.81	1.00										
Y	0.02	0.96	-0.60	0.64	0.35	0.94	0.47	0.87	0.65	0.44	0.86	0.50	0.63	0.57	0.56	0.90	1.00									
Zr	0.07	0.41	-0.33	0.01	0.31	0.41	0.85	0.46	-0.01	-0.18	0.47	-0.05	-0.03	0.41	0.39	0.50	0.44	1.00								
Ba	0.24	0.85	-0.72	0.46	0.16	0.85	0.43	0.90	0.51	0.33	0.89	0.59	0.51	0.54	0.60	0.95	0.96	0.49	1.00							
Hf	0.05	0.43	-0.26	-0.03	0.01	0.27	0.56	0.67	-0.24	-0.42	0.15	-0.36	-0.32	0.87	0.80	0.64	0.45	0.76	0.46	1.00						
Ni	-0.45	0.13	0.16	0.28	0.73	0.16	0.11	-0.32	0.33	0.12	-0.10	-0.07	0.39	-0.23	-0.35	-0.41	-0.10	-0.01	-0.28	-0.22	1.00					
Zn	-0.83	0.65	0.38	0.93	0.68	0.60	0.35	0.13	0.74	0.69	0.23	-0.16	0.59	0.22	-0.05	0.17	0.46	-0.09	0.24	0.06	0.27	1.00				
Pb	0.06	-0.64	0.40	-0.35	-0.62	-0.72	-0.86	-0.44	-0.44	-0.24	-0.76	-0.30	-0.46	-0.19	-0.17	-0.49	0.63	0.87	0.63	-0.46	-0.24	-0.13	1.00			
Sc	-0.55	0.82	-0.01	0.98	0.65	0.85	0.38	0.34	0.94	0.87	0.63	0.32	0.86	0.14	-0.01	0.42	0.73	0.00	0.57	-0.03	0.16	0.88	0.35	1.00		
Co	-0.77	0.57	0.26	0.86	0.94	0.62	0.40	-0.10	0.84	0.72	0.32	0.08	0.80	-0.15	-0.36	-0.08	0.34	0.00	0.12	-0.21	0.72	0.80	-0.38	0.77	1.00	
Th	-0.29	0.32	0.08	0.45	0.52	0.51	0.75	-0.04	0.54	0.65	0.67	0.28	0.51	-0.34	-0.40	0.14	0.33	0.48	0.35	-0.03	-0.05	0.24	-0.68	0.45	0.38	1.00

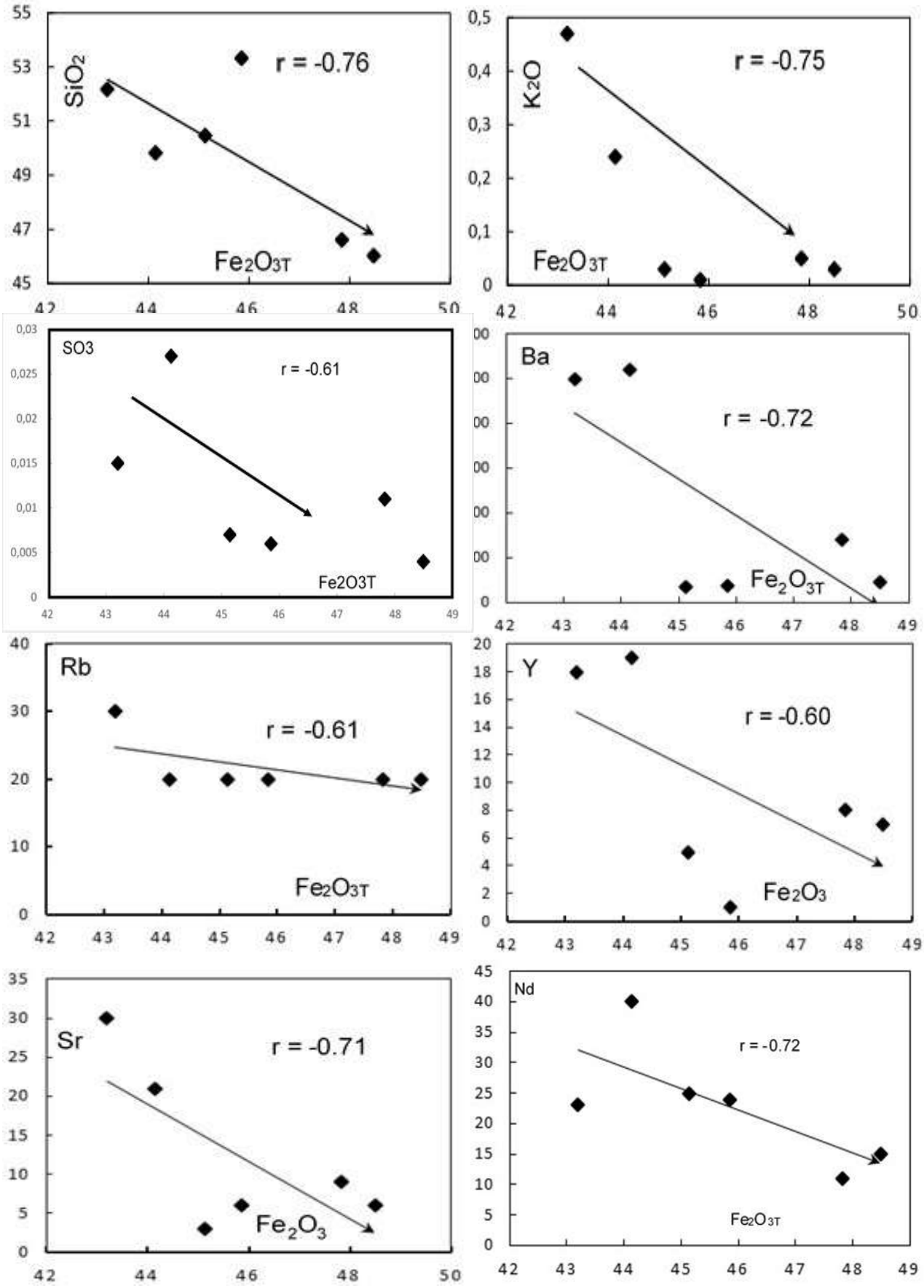

Fig. 3. Selected Harker diagrams showing negative correlation with $Fe2O3_T$

2) Trace elements

Concentrations of trace elements in the bulk samples are shown in Table 1, no significant enrichments were observed. Variations in some enriched transition elements are as follows: V (7 – 132 ppm), Zn (16 – 103 ppm), Ni (18 – 58 ppm), Cr (16 – 26 ppm) and Cu (6 – 20 ppm). These elements are commonly used as indicators of direct volcanogenic hydrothermal input in chemical precipitates [28]. The Pout Njouma iron deposits are depleted in high field strength elements (HFSE) such as Sc, Y, Zr that vary from 2.1 – 11.6 ppm, ≤ 19 ppm, 5 – 36 ppm respectively (Table 2). The contents of large ion lithophile elements (LILE) such as Rb (20 to 30 ppm), Sr (3 to 30 ppm) are relatively elevated with Ba (33 to 520 ppm) showing high values of concentration in sample PD13 (Ba: 520 ppm) and sample PD15 (Ba: 499 ppm). In Pearson's correlation matrix (Table 2) and binary plots (Fig. 3), Fe_2O_{3T} shows strong negative correlation with Sr (r = -0.71), Y (r =-0.60), Rb (r = -0.613), Ba (r =-0.72), and Nd (r = -0.73).

3) Rare earth elements

Rare earth element (REE) distributions in the Pout Njouma iron occurrence bulk samples are shown in Table 2. The total rare earth elements (ΣREE) ranges from 44.65 to 121.43 ppm with an average value of 86.72 ppm. The degree of light rare earth elements (LREE) enrichment relative to heavy rare earth elements (HREE) is presented as the ratios of PAAS-normalized $(La/Yb)_N$ ratio and $(Tb/Yb)_N$ ratio. On the normalized Post-Archaean Australian Shale (PAAS; [52]) diagram as observed in figure 4, the REE patterns show a slight enrichment in light REE (La_N/Yb_N = 0.89 - 8.6) relative to the heavy REE (Tb_N/Yb_N = 0.83 - 6.06). $Eu/Eu^* = Eu_N/(0.67Sm_N + 0.33Tb_N)$ after [53] and $Ce/Ce^* = \log[Ce_N/(La_N \times Nd_N)^{1/2}]$ according to [54] are used to evaluate Eu and Ce anomalies values respectively (Table 2). Accordingly, the analyzed samples display a positive Eu anomaly (Eu/Eu* = 1 - 1.45) and a poor to near null negative Ce anomaly (Ce/Ce* = 0.19 - 0.52). The degree of positive Eu anomaly decreases with increasing ΣREE. Sample with the least ΣREE (44.65 ppm) is characterized by the largest positive Eu anomaly (1.52; Table 1). One sample (PD13) with a relatively high Al_2O_3 content (2.81%) has a very high ΣREE (121.43 ppm; Table 1), suggesting that REEs are partly derived from a detrital component (Al- bearing phase).

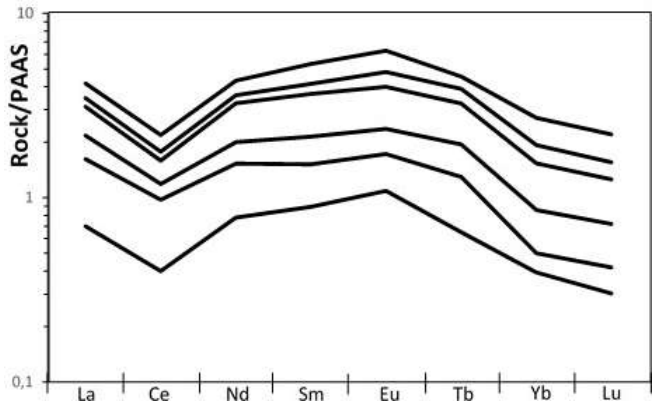

Fig. 4. PAAS [52] normalized REEs for Pout Njouma iron mineralization.

V. Discussion

A. Lithology

Lithologically, Pout Njouma area is made up of banded iron formation (BIF), magnetite- gneiss and magnetite- quartzite (Fig. 1b). Petrographic examination of the studied BIFs shows the paragenesis range from greenschist facies (Mgt + Qtz ± Pl + Ser ± Lm) to the amphibolite facies (Mgt + Qtz + Hbl ± Pl + Ser ± Lm). According to [29], [34] and [55], BIF and the associated rock units within the Nyong series of Ntem complex are metamorphosed from greenschist to granulite metamorphic facies conditions. The rocks identified in this study confirm the fact that the Nyong unit is composed of banded series [56], with characteristics of the greenstone belt facies of rocks [43] including basic and ferriferous or sterile quartzitic rocks, orthogneisses and metaquartzites, with a dominance of biotite- amphibole gneiss, pyrigarnite and magnetite- bearing gneiss [23]. Other areas within the Nyong unit display similar lithology: Kopongo (quartzite rich magnetite-martite [31]), Kpwa–Atog Boga (BIF and Garnet-gneiss [35]), Ngovayang (BIF, gneiss and granitoids, metabasites pyroxenites, amphibolites and ferruginous quartzites [56]), Elom (BIF, gneiss, charnokite, high k-granite and gabbro [27]).

B. Nature and Protoliths

Based on silica content (average: 49.73% SiO_2) compared to Fe content (average: 45.77% Fe_2O_{3T}), the Pout Njouma iron deposits fall into the group of oxide facies [8], [57] and [58] with magnetite as dominant mineral. This result is in accordance with the majority of iron deposits in Cameroon where either hematite or magnetite are dominant minerals. High contents of SiO_2 and Fe_2O_3 in the studied iron formations indicate the purity of the chemical precipitates while the high silica contents alone are also attributable to the high metachert or quartz constituents of the iron formation.

The studied rocks have stable features of LILE and their geochemical signature can be used to identify their protolith. Therefore, the nature of the sedimentary sources can be constrained using the geochemical signatures of these rocks. Based on the diagram log (Fe_2O_{3T}/K_2O) vs. log (SiO_2/Al_2O_3) of [59] represented in figure 5a, the Pout Njouma iron deposits fall into the field of Fe-sand, suggesting their provenance from the sediments of Fe-sand type. The Fe-sand type sediments as protoliths of BIFs are also reported in the Messondo area [36], while [34] recorded Fe-shale and shale to Fe-shale as source of provenance of Kpwa-Atog Boga iron formations.

C. Detrital input into BIFs

The patterns of element abundances preserved in ancient chemical sediments can be used to constrain the influence of seawater, hydrothermal, biogenic and detrital sources on the sediment composition. By this, high Al_2O_3 and TiO_2 contents are considered indicators of detrital influx during BIF deposition [60], [61]. However, elevated Al_2O_3 and TiO_2, MgO, CaO and K_2O are regularly present in sediments [25].

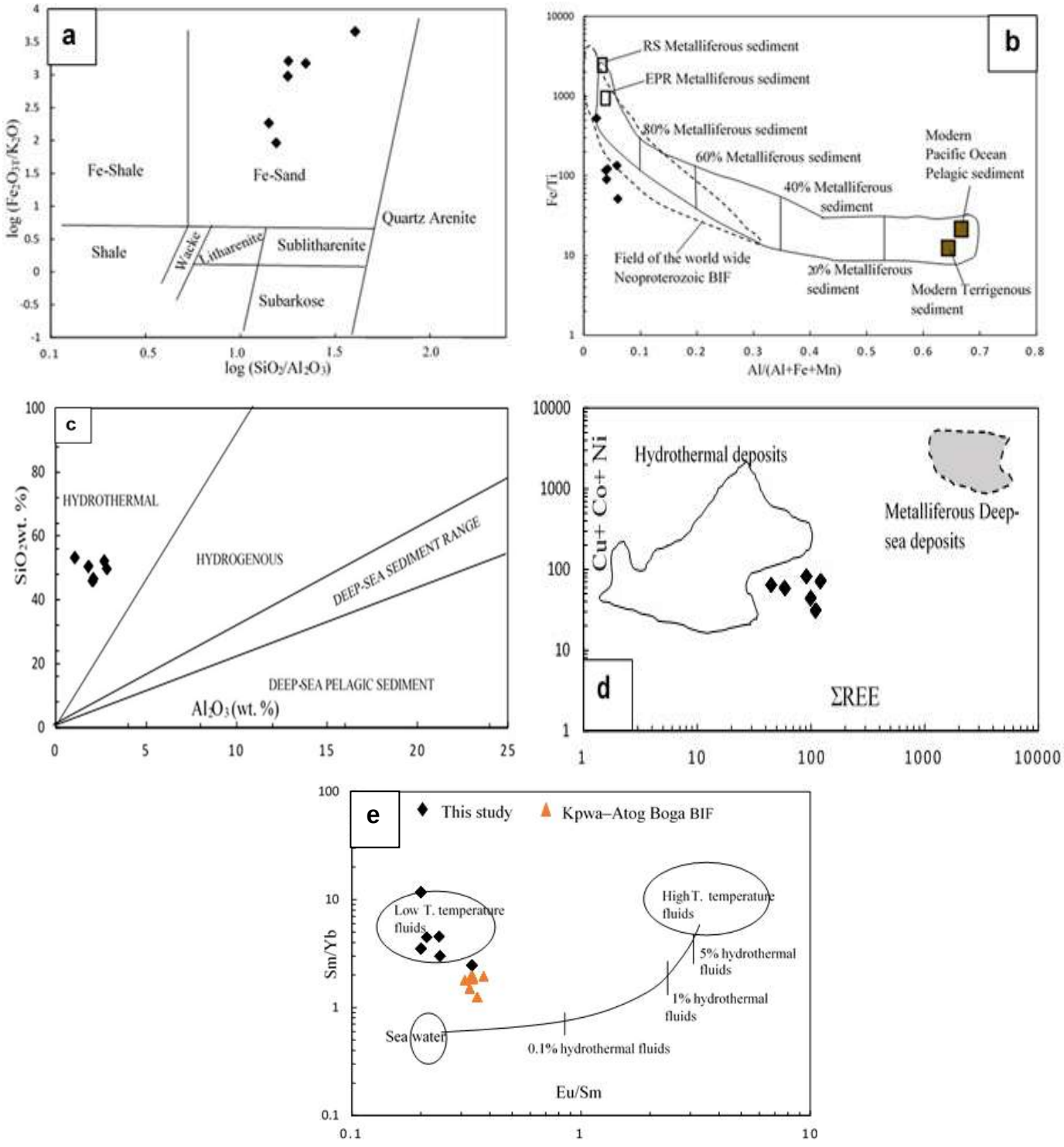

Fig. 5. Composition of Pout Njouma iron occurrence. (a): plot of log (Fe_2O_{3T}/K_2O) vs. log (SiO_2/ Al_2O_3) adapted from [59] showing the chemical composition. (b): Discriminative diagram Fe/Ti vs. Al/(Al + Fe + Mn) after [62]. The dotted outline defines the worldwide Neoproterozoic BIFs field and the black outline represents ideal mixture of metalliferous and terrigenous sediments, between metalliferous sediments and pacific ocean pelagic sediments. EPR: East Pacific Rise, and RS: Red Sea. (c): SiO_2 vs. Al_2O_3 discrimination diagram indicating the hydrothermal affinity of Pout Njouma iron mineralization. (d): Plot of Pout Njouma iron samples in the diagram Co + Ni + Cu vs. ΣREE of [63]. (e): Plot of the composition of the studied rocks in the diagram Sm/Yb vs. Eu/Sm modified after [64]. Data source: Mean composition of high-temperature (> 350°C) hydrothermal fluids [65], low-temperature hydrothermal solutions [66], and Pacific seawater [67].

Estimates indicate that typical chemical sediment enriched in Mn and Fe serve as partial hydrothermal proxies, but the addition of detrital or volcanic materials results in dilution and enrichment of Ti, Al and Zr [68]. Table 1 shows that the Pout Njouma iron occurrence are relatively enriched in Al_2O_3 (1.05 to 2.81%) and TiO_2 (0.087 - 0.86 %). Thus, the incorporation of terrigenous sediments input in the deposition of the Pout Njouma iron formations is suggested by the relative elevated values of Ti and Al and the strong positive correlation (r = -0.74) between Al_2O_3 with TiO_2.

This positive correlation between Al_2O_3 and TiO_2 has equally been reported in different BIFs in Cameroon: Kopongo [31] and around the world [60], [63], [69]-[71].

Barrett (1981) proposed the use of Fe/Ti versus Al/ (Al + Fe + Mn) binary diagram to assess the relative input of terrigenous and hydrothermal fractions in pelagic sediments. On this diagram (Fig. 5b), the Pout Njouma iron formations cluster into the field of East Pacific Rise (EPR) metalliferous sediment closer to 80% metalliferous sediment. This implies that the studied iron deposits are predominantly of hydrothermal origin with slight input of continental crustal material. The east pacific hydrothermal origin of BIFs is reported for the majority of iron deposits in Cameroon (Zambi area [28]; Kouambo [29]; Bienkop [24]; Kopongo [31]; Kpwa-Atog Boga [34]; Gouap [35]; Messondo area [36]. A Red sea deposit is recorded in Elom [27] while red sea deposit to East pacific rise deposit is reported in Meyomessi [30]. Furthermore, [21] suggested that the Metzimevin iron deposit is the result of hypogene leaching of gangue minerals from, and further hematitization of, an itabirite protore. Pure hydrothermal deposits contain very little Al and have high Al/Ti ratios [73].

Trace elements such as Zr, Hf, Y, Rb and Sr are commonly derived from weathering of crustal felsic rocks, whereas Cr, Ni, Co, V and Sc commonly have a mafic source [74], [75]. Table 1 displays significant positive correlations of Al_2O_3 with LILE, HFSE and transition metals: V (r = 0.69), Cr (r = 0.55), Rb (r = 0.46), Sr (r = 0.77), Y (r = 0.95), Zr (r = 0.41), Ba (r = 0.84), Hf (r = 0.42), Zn (r = 0.64), Sc (r = 0.82), and Co (r = 0.56). This could also indicate a contribution of clastic materials and further suggests that these detritus might have been derived from weathering of both felsic and mafic (bimodal) sources. This is similar to the results obtain by [31] where the iron occurrence of Kopongo reveals relatively average values of Ti, Al and Zr suggesting a low contribution of detrital materials.

D. Source of chemical components / origin of Pout Njouma iron deposits

The source of Fe and Si in BIFs is typically attributed to (i) anoxic weathering on continent [76], (ii) sea floor volcanic activity or hydrothermal vent activity or ocean floor within their depositional basins [16], [77], [78] or (iii) hydrothermal leaching of pre-existing sediments [79]. It is however on the basis of the differences in the mineralogical, chemical and isotopic composition that methods have been proposed for distinguishing between seawater, hydrothermal, biogenic and detrital sources on BIF genesis.

The Si/Al ratio is used in the study of sedimentary rock to distinguish between hydrothermal Fe-Mn crusts, rich in Si and characterized by a Si/Al ratio > 5.1, and hydrogenous Fe-deposits, whose typical Si/Al ratio is 3. The average Si/Al ratio of the studied BIFs is 26.8 pointing to hydrothermal origin. The hydrothermal source for the Pout Njouma iron deposits is confirmed by [68] who equally suggested that hydrothermal metal- rich deposits could be distinguished from hydrogenous deposits on the basis of the relative abundance of SiO_2 and Al_2O_3. SiO_2 and Al_2O_3 diagram (Fig. 5c) plotting of Pout Njouma iron samples showed that, they fall into the hydrothermal field. This results suggests an important contribution (in the volume) of the components of hydrothermal origin during the deposition of studied formations and further confirms the consensus that the source of iron in Precambrian iron formations was in hydrothermal fluids that vented into the deep ocean during submarine volcanism [3]. The positive correlations between Al_2O_3 and TiO_2 (r = 0.75), Na_2O (r = 0.53), K_2O (r = 0.75), MnO (r = 0.78), MgO (r = 0.57) and CaO (r = 0.97; Table 2) suggest a common origin for these elements, which were likely present in detrital particles. Hydrothermal origin has also reported in other Cameroon BIFs: Zambi [27], Elom [28], Kouambo [29], Bienkop [24], Meyomessi [30], Kpwa–Atog Boga [34], Gouap [35], Messondo [36]. This however differs from the hydrogenous origin displayed by the Mafe silicate BIF facies [80], pointing to seawater as the main source of chemical elements.

Transition metals (e.g., Cr, Co, Ni, Cu, and Zn) are good diagnostic tracers of the chemical composition of their sources, thus the hydrothermal origin of Pout Njouma iron mineralizations is further confirm by Co + Ni + Cu vs. ΣREE diagram proposed by [63]. This diagram is used to recognize the nature of the origin of these elements in BIFs [61], [70], [81] so as to distinguish between hydrothermal and metalliferous-deep sea deposits, because modern seawater wedge fluids are characterized by Cu, Ni, and Co enrichment. Plot of studied materials on Co + Ni + Cu vs. ΣREE diagram (Fig. 5d) cluster close to the hydrothermal deposits field and far from the metalliferous-deep sea deposits field, suggesting that the Si and Fe components of the studied rocks were formed by hydrothermal fluids. This result coincides with the studies of [29] in Elom, Changyi BIFs [61], and Kpwa-Atog Boga BIFs [34]. Furthermore, strong positive Eu anomalies have been attributed to high-temperature (> 250°C) hydrothermal fluids, while weak to no Eu anomaly indicates fluids of low-temperature (< 200°C) [60]. Thus, it is possible that the weak positive Eu anomalies (Eu/Eu*=1.9-1.45) observed in figure 4 is inherited from low-temperature hydrothermal fluids. Bau and Möller (1993) reported that the decrease in the positive Eu anomaly is the result of the lowering of the temperature of the hydrothermal solutions, as a reflection of decreasing upper mantle temperature. Moreover, the fraction of seawater and hydrothermal fluids can be assessed using the Sm/Yb vs. Eu/Sm diagram of [64]. On this diagram (Fig. 5e), the Pout Njouma iron samples occupy the field of Low-T temperature fluids. This suggests that low-temperature hydrothermal fluids (< 200°C) have occurred during the deposition of the studied BIFs. This result is different with the one obtained in Kpwa-Atog Boga, Kouambo, Penge and Changyi BIFs that fall near the fields of Low-T temperature fluids and seawater, indicating that mixing of seawater and less amount (< 0.1%) of low-temperature hydrothermal fluids (< 200°C) might have occurred during their deposition.

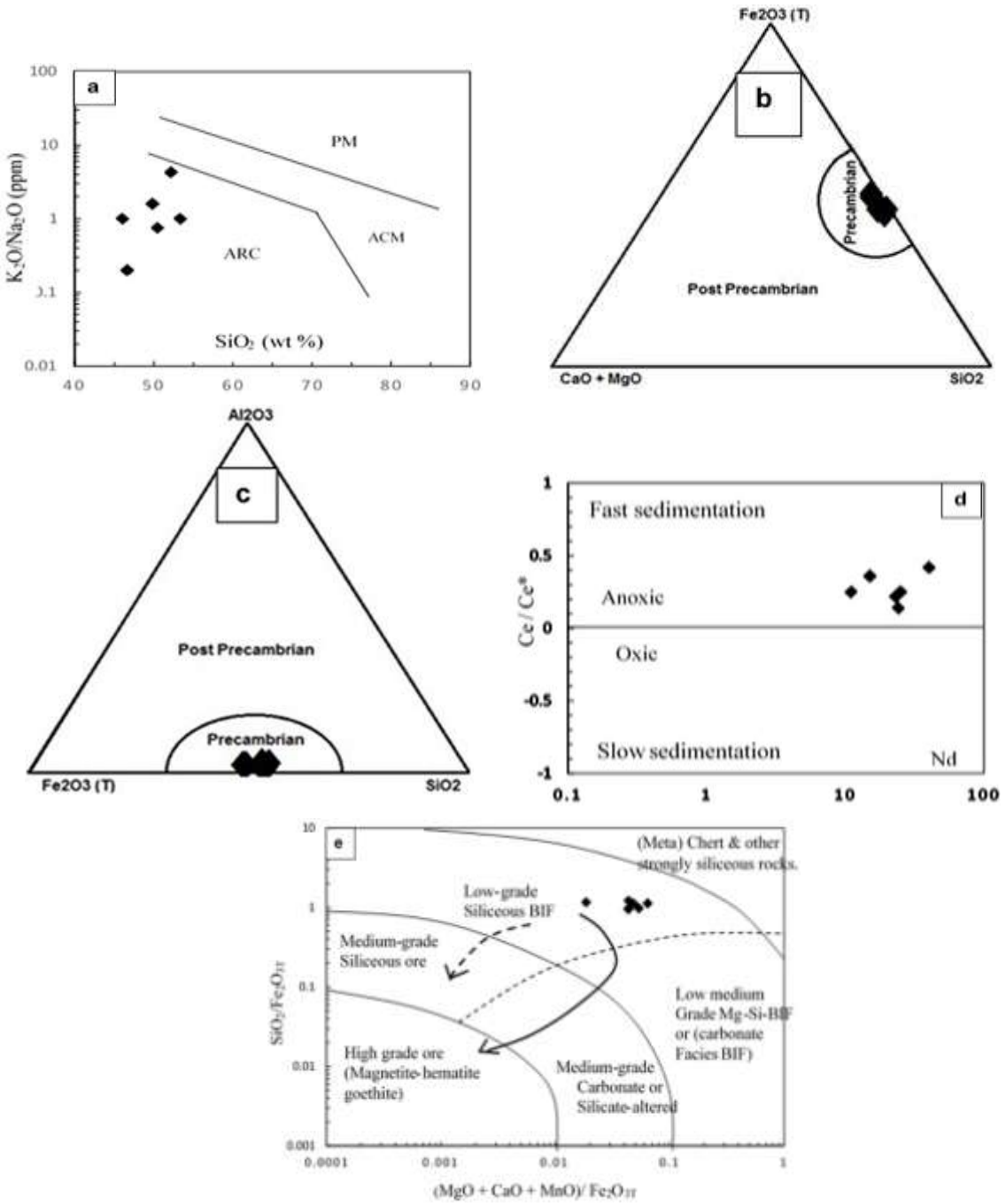

Fig. 6. (a): K_2O/Na_2O vs. SiO_2 diagram after [83] discriminating the tectonic settings of Pout Njouma iron deposits: ARC = oceanic island-arc margin, ACM = active continental margin, and PM = passive margin. (b, c): Composition of Pout Njouma iron occurrence plotted in the diagram of [84] and [85] respectively. (d): Plot of Ce anomaly versus Nd concentrations. The dividing line between anoxic and oxic is after [86]). (e): Discrimination diagrams for the whole rock geochemistry of the Pout Njouma BIFs, displaying major oxide ratios $(MgO + CaO + MnO)/ Fe_2O_{3total}$ versus SiO_2/Fe_2O_{3total} [87] with discrimination fields and arrows illustrating the low to medium-grade siliceous ore type and the alteration trends with the MgO + CaO + MnO- rich and-poorstage.

E. Depositional Setting

The tectonic setting of sedimentary rocks can be inferred from major elemental data [88] and [89]. It predominately exhibits the nature and proportion of their detrital components and the bulk composition reflects the tectonic settings of the basin [83] and [90]. Roser and Korsch (1986) proposed a discriminating diagram using (K_2O/Na_2O) vs SiO_2 to establish various tectonic settings of clastic rocks. Plotted on this diagram (Fig. 6a), all the samples fall into the field of oceanic island arc margin (ARC), suggesting they were deposited in the oceanic island arc margin setting. The same depositional setting has been observed for the Messondo BIFs, whereas the Kpwa-Atog Boga BIFs have been deposited in an active continental margin.

On Fe_2O_{3T} - CaO + MgO - SiO_2 of [84] and Al_2O_3 - SiO_2 - Fe_2O_{3T} after [85] ternary plots, studied materials indicate a Precambrian affinity suggesting that the Pout Njouma iron deposits derived from Precambrian rocks (Fig. 6b, 6c). The Precambrian iron formations have low Al_2O_3, TiO_2, P_2O_5, CaO and MgO contents relative to post-Precambrian

deposits [84], [85]. This result comforts the studies of [31]), [34] and [36] who also reported a Precambrian affinity for the iron mineralization in Kopongo, Kpwa-Atog Boga and Messondo respectively.

The Ce anomaly (Ce/Ce* = 0.19-0.52) is calculated to investigate for the conditions of the formation of the studied iron deposits. The values are plotted on the Ce/Ce* vs. Nd concentrations as from the diagram of [86]. The plot shows that the Pout Njouma iron rocks were deposited under anoxic conditions accompanied by fast sedimentation (Fig. 6d). Similar result is obtained for the Messondo BIFs [36].

E. Iron Potential

Angerer et al. (2012) introduces a discrimination diagram to distinguish various ore grades by using major oxide ratios such as SiO_2/Fe_2O_{3total} and $(MgO + CaO + MnO)/Fe_2O_{3total}$ to identify carbonate- or silicate- rich zones in BIF and illustrate the evolution of hypogene hydrothermal alteration zones through time. In this diagram (Fig. 6e), the analyzed samples have been plotted in the low-grade siliceous ore, suggesting the Pout Njouma BIFs host low-grade siliceous ore. This is in accordance with the study of [35] where the magnetite- rich BIF samples (amphibole and amphibole-pyrite BIF) from Gouap were plotted in the field of low-grade siliceous BIF. In contrast the enriched BIF samples (hematite- martite BIF) from Gouap were plotted along the boundaries of medium-grade and low-grade siliceous ore.

Furthermore, the potential of iron ore mineralization is generally viewed using the iron percentage [24]. According to [91], exploited iron ores can be divided into three basic classes based on the Fe content: high-grade iron ores with a total Fe content above 65%, medium-grade ores with varied Fe contents in the range between 52 and 65%; and low-grade ores with Fe contents below 52%. Based on the classification it is clear that the iron mineralization of the Pout Njouma area is of low grade (average Fe = 45.77%) by global standards but largely remain in the extracting range since the Fe_2O_3 percentage vary between 43.19 to 48.49%. Thus the studied iron formations corresponds to depleted iron ore that contain 30 to 50% Fe [92]. Similar results were obtained from Zambi deposit [27], Nkout deposit [33], Kouambo deposit [29] and Messondo deposit [36].

F. Comparison with the others BIFs

Average oxide contents of Pout Njouma iron formations is compared with those of Algoma, Lake Superior, Nigeria, Mballam, Mayo Binka, Elom and Messondo as recorded in Table 3. SiO_2 and Fe_2O_3 in the most BIFs show significant enrichment except in Mballam (Fe_2O_3 = 60.75%) and Mayo Binka (Fe_2O_3 = 82.31%) where Fe shows very high elevated values compared to SiO_2 contents (Mballam: SiO_2 = 23.53%, Mayo Binka: SiO_2 = 11.91%). The data also show low concentration of Al_2O_3, TiO_2, CaO and MnO, which infers the non-volcanogenic origin. Very low concentrations of Na_2O and K_2O values also substantiate the above observation. The average alumina concentrations (2.07%) of the studied BIFs it very smaller than the one of Mballan (9.02%). It is almost similar with Al_2O_3 (3.06%) of Algoma- type, Lake Superior- type (1.45%), Messondo BIFs (1.12%). Whereas it is slightly greater than that of the Nigeria BIFs (0.28%), Mayo Mbinka (0.24%) and Elom (0.48%). When plotted against the respective oxides for selected BIFs (Fig. 7), SiO_2 and Fe_2O_3 in all the BIFs show significant high proportions except in Mballam and Mayo Binka where Fe shows very elevated values compared to SiO_2. There is a significant variation in Al_2O_3, MnO, CaO, Na_2O, K_2O and P_2O_5 proportions that are moderate in the study area BIF.

VI. Conclusion

The Pout Njouma area is located within the Paleoproterozoic Nyong unit which belongs to the Ntem Complex. Lithologically and based on mineralogical composition, the Pout Njouma area is made up of magnetite- gneiss, magnetite- quartzite and BIF. These rocks display microband texture and granoblastic microstructures. Magnetite- gneiss and magnetite- quartzite display the parageneses of greenschist facies, while banded iron formations show the parageneses of greenschist to amphibolite facies. The Pout Njouma iron deposits belong to the oxide facies, with magnetite and quartz being the common predominant minerals while sericite and limonite occur as accessory minerals.

Fe_2O_3 and SiO_2 are the most dominant major elements and the two elements represent 95.05 % of the total bulk rock composition, while the others represent 4.95%, indicating the purity of the chemical precipitates. The strong negative correlation between Fe_2O_{3T} and SiO_2 suggests the incorporation of Fe_2O_3 and SiO_2 in different mineral phases.

A sedimentary origin with a high contribution of hydrothermal fluids and low input of detrital materials has been suggested for the Pout Njouma iron deposits. This geochemical signature is supported by the presence of Al_2O_3 and TiO_2 in the samples indicating that crustal materials contributed insignificantly to their chemical precipitation.

The absence of a large positive Eu anomaly in the studied Pout Njouma iron mineralization indicates an important role of low-temperature hydrothermal solutions. Sm/Yb vs. Eu/Sm diagram supports this interpretation through the plot of all data into the Low-temperature hydrothermal fluids field suggesting that low-temperature hydrothermal fluids (< 200°C) have occurred during the deposition of these BIFs.

Pout Njouma iron deposit is of low grade siliceous ore (average Fe = 45.77 wt %) by global standards but largely remain in the extracting range since the Fe_2O_3 percentage varies between 43.19 to 48.49%, and it corresponds to the depleted iron ore. The Pout Njouma iron deposits derived from Precambrian rocks, which were deposited in an oceanic island-arc margin (ARC) setting where conditions were anoxic and fast sedimentation.

The average chemical composition of Pout Njouma BIFs is compared with other studied BIFs and the result shows low concentration of Al_2O_3, TiO_2, CaO and MnO, which infers the non-volcanogenic origin.

TABLE IIVI
COMPARISON OF THE AVERAGE CONCENTRATION OF MAJOR ELEMENTS FROM POUT NJOUMA BIFS WITH OTHERS BIFS.

Major oxides	Mayo Binka BIFs [21]	Mballam BIFs [22]	Algoma type BIFs [93]	Lake Superior type BIFs [93]	Nigeria BIFs [93]	Elom BIFs [28]	Messondo BIFs [36]	Pout Njouma (This study)
SiO_2	11.91	23.53	50.58	49.13	57.66	39.98	47.80	49.73
Al_2O_3	0.24	9.02	3.06	1.45	0.28	0.48	1.12	2.07
Fe_2O_3	82.31	60.75	42.62	46.33	42.02	58.19	48.90	45.77
MnO	0.52	0.03	0.14	0.76	0.06	0.07	0.03	0.09
MgO	0.16	0.03	1.56	1.29	0.01	0.06	0.21	1.58
CaO	0.01	0.02	1.54	1.64	0.02	0.02	0.2	0.39
Na_2O	1.16	0.02	0.32	0.12	0.01	0.01	0.59	0.09
K_2O	1.01	0.12	0.59	0.15	0.02	0.08	0.07	0.16
TiO_2	0.01	0.28	0.09	0.02	0.02	0.03	0.11	0.43
P_2O_5	1.98	0.17	0.21	0.06	0.05	0.08	0.22	0.14
SO_3	NA	NA	0.3	0.02	NA	NA	<0.01	0.01

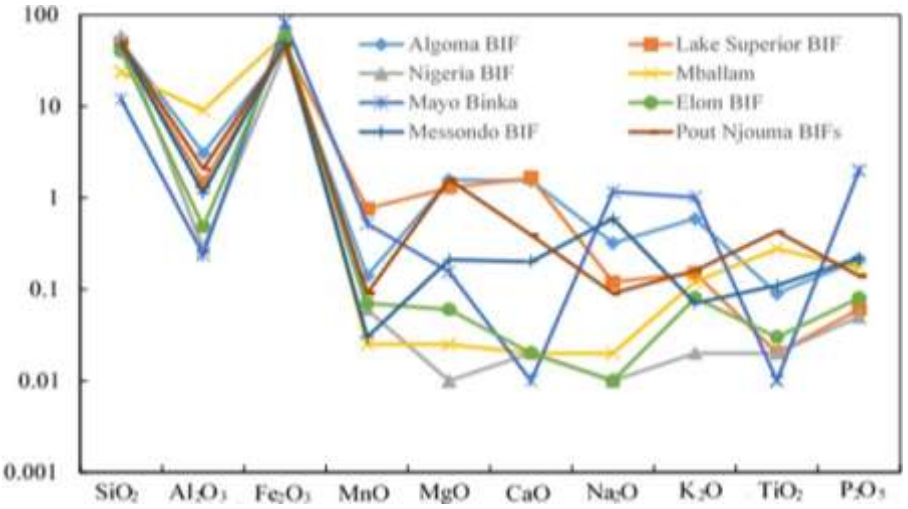

Fig. 7. Chemical variation in composition of major elements of Pout Njouma's BIFs with the documented BIFs

REFERENCES

[1] Klein, C., (2005). Some Precambrian banded-iron formation (BIFs) from around the world: their age, geologic setting, mineralogy, metamorphism, geochemistry and origin. Am. Miner. 90, 1473–1499.

[2] Lewy, Z., (2012). Banded Iron Formations (BIFs) and Associated Sediments Do Not Reflect the Physical and Chemical Properties of Early Precambrian Seas. International Journal of Geosciences, Vol. 3, No. 1, pp. 226-236. doi:10.4236/ijg.2012.31026

[3] Bekker, A., Slack, J.F., Planavsky, N., Krapež, B., Hofmann, A., Konhauser, K.O., and Rouxel, O.J., (2010). Iron formation: The sedimentary product of a complex interplay among mantle, tectonic, oceanic, and biospheric processes. Economic Geology and the Bulletin of the Society of Economic Geologists, v. 105, p. 467–508, doi:10.2113/gsecongeo.105.3.467.

[4] Huston, D.L., Logan, G.A., (2004) Barite, BIFs and bugs: evidence for the evolution of the Earth's early hydrosphere. Earth Planet. Sci. Lett. 220, pp. 41– 55.

[5] Holland, H.D., (2005). Sedimentary mineral deposits and the evolution of Earth's nearsurface environments. Economic Geology and the Bulletin of the Society of Economic Geologists, v. 100, p. 1489–1509, doi:10.2113/gsecongeo .100.8.1489.

[6] Isley, A.E., (1995). Hydrothermal plumes and the delivery of iron to banded iron formations. Journal of Geology, 103, 169-185. doi:10.1086/629734.

[7] Slack, J.F. and Cannon, W.F., (2009). Extraterrestrial Demise of banded irons formations 1.81 billion years ago. Science, 37; 1011-1014.

[8] James, H.J., (1954). Sedimentary Facies of Iron Formation. Economic Geology, 49, 235-293. https://doi.org/10.2113/gsecongeo.49.3.235.

[9] Gross, G.A., (1980). A classification of iron formations based on depositional environments. Can. Mineral. 18, 215–222.

[10] Gross, G.A., (1965). Geology of Iron Deposits in Canada, Volume 1. General Geology and Evaluation of Iron Deposits, Geological Survey of Canada Economic Report, 22p.

[11] Misra, K., (1999). Understanding Mineral Deposits. Kluwer Academic Publishers, 845p.

[12] Gross, G.A., (1983). Iron-Formation in Fold Belts Marginal to the Ungava Craton. In: Trendall, A.F. and Morris, R.C., Eds., Iron Formation: Facts and Problems, Elsevier, Amsterdam, 253-294.

[13] Jébrak, M. et Marcoux, E., (2008). Géologie des ressources minérales, Association géologique du Canada. Ressources naturelles et Faune Québec, Gouvernement du Québec 667p.

[14] Guilbert, J.M. and Park, C.F., (1986). The Geology of Ore Deposits. Freeman and Co., New York. 985 pp.

[15] Garrels, R.M., (1960). Mineral equilibrium at low temperature and pressure. Harper and Brothers, New York. I Vol., 225 pages.

[16] Trendall, A.F., Blockley, J.F., (1970). The iron formation of the Precambrian Hamersley Group, Western Australia: Geological Survey of Western Australia Bulletin 119. Geological Survey of Western Australia Bulletin Perth.

[17] Trendall, A. F., (1973). Precambrian iron-formation of Australia. Econ. Geol., 68, 1023–1034.

[18] Clout, J.M.F. and Simonson, B.M., (2005). Precambrian iron formations and iron formation-hosted iron ore deposits. In Hedenquist, J. W., Thompson, J. F. H., Goldfarb, R. J. and Richards, J. P. (eds.) Economic geology 100th anniversary volume. Society of Economic Geologists Inc., Littleton, 643–679.

[19] Laberge, G.L., (1966). Altered pyroclastic rocks in iron-formation in the Hamersley Range, Western Australia. Economic Geology, vol. 61, p. 147-161.

[20] Pickard, A.L., (2002). SHRIMP U-Pb zircon ages of tuffaceous mudrocks in the Brockman iron formation of the Hamersley Range, Western Australia. Australian Journal of Earth Sciences. 49 (3) 491-507.

[21] Suh, C. E., Cabral, A., Shemang, E. M., Mbinkar, L. and Mboudou, G. G. M., (2008). Two contrasting iron-ore deposits in the Precambrian mineral belt of Cameroon, West Africa. Explor. Min. Geol., 17, 197–207.

[22] Nforba, M.T., Kabeyene, K.V., Suh, C.E., (2011). Regolith geochemistry and mineralogy of the Mbalam itabirite-hosted iron ore district, southeastern Cameroon. Open J. Geol. 1, 17–36.

[23] Chombong, N.N., Suh, C.E., (2013). 2883 Ma commencement of BIF deposition at the northern edge of Congo craton, southern Cameroon: new zircon SHRIMP data constraint from metavolcanics. Episodes. 36:47-57.

[24] Ilouga, D.C.I., Suh, C.E., Ghogomu, R.T., (2013). Textures and rare earth elements composition of banded iron formations (BIF) at Njweng, Mbalam iron ore district, southern Cameroon. Int. J. Geosci. 4, 146–165.

[25] Ilouga, D.C.I., Ndong Bidzang, F., Ziem A Bidias, L.A., Olinga, J.B., Tata, E., Minyem, D., (2017). Geochemical Characterization of a Stratigraphic Log Bearing Iron Ore in the Sanaga Prospect, Upper Nyong Unit of Ntem Complex, Cameroon. Journal of Geosciences and Geomatics, 2017, Vol. 5, No. 5, 218-228. DOI:10.12691/jgg-5-5-1.

[26] Anderson, K.F.E., Frances, W., Rollinson, G.K., Charles, J.M., (2014). Quantitative mineralogical and chemical assessment of the Nkout iron ore deposit, Southern Cameroon. Ore Geol. Rev. 62, 25–39.

[27] Ganno, S., Ngnotue, T., Kouankap, N.G.D., Nzenti, J.P. and Notsa, F.M., (2015a). Petrology and geochemistry of the banded iron-formations from Ntem complex greenstones belt, Elom area, southern Cameroon: Implications for the origin and depositional environment. Chem. Erde-Geochem., 75, 375–387.

[28] Ganno, S., Moudioh, C., Nzina Nchare, A., Kouankap Nono, G.D. and Nzenti, J.P., (2015b). Geochemical fingerprint and iron ore potential of the siliceous itabirite from Palaeoproterozoic Nyong series, Zambi area, southwestern Cameroon. Resour. Geol., 66, 71–80.

[29] Ganno, S., Njiosseu, T.E.L., Kouankap, N.G.D., Djoukouo, S.A.P., Moudioh, C., Ngnotué, T. and Nzenti, J.P., (2017). A mixed seawater and hydrothermal origin of superior-type banded iron formation (BIF)-hosted Kouambo iron deposit, Palaeoproterozoic Nyong series, southwestern Cameroon: Constraints from petrography and geochemistry. Ore Geol. Rev., 80, 860–875.

[30] Ganno, S., Tsozué, D. Kouankap, N.G.D, Tchouatcha, M.S., Ngnotué, T., Takam, R.G. and Nzenti, J.P., (2018). Geochemical constraints of iron from the Archaen Ntem Complex (Congo Craton) in the Meyomessi Area, Southern Cameroon. Resource Geology. DOI: 10.1111/rge. 12172.

[31] Mbang Bonda, B.M., Etame, J., Kouske, A.P., Bayiga, E.C., Ngon Ngon, G.F., Mbaï, S.J. Gérard, M., (2017), Ore Texture, Mineralogy and Whole Rock Geochemistry of the Iron Mineralization from Edea North Area, Nyong Complex, Southern Cameroon: Implication for Origin and Enrichment Process. International Journal of Geosciences, 8, 659-677. https://doi.org/10.4236/ijg.2017.85036.

[32] Tessontsap Teutsong, Tomaso, R.R., Bontognali, Ndjigui, P.D., Vrijmoed, Teagle, D., Cooper, M., Vance, D., (2017). Petrography and geochemistry of the Mesoarchean Bikoula banded iron formation in the Ntem complex (Congo craton), southern Cameroon: implications for its origin. Ore Geol. 80, 267–388.

[33] Ndime, E.N., Ganno, S., Soh Tamehe, L., Nzenti, J.P., (2018). Petrography, lithostratigraphy and major element geochemistry of Mesoarchean metamorphosed banded iron formation-hosted Nkout iron ore deposit, north western Congo craton, Central West Africa. J. Afr. Earth Sci. 148.

[34] Soh Tamehe, L., Nzepang, T.M., Chongtao, W., Ganno, S., Ngnotue, T., Kouankap, N.G.D., Simon, S.J., Zhang, J., Nzenti, J.P., (2018). Geology and geochemical constrains on the origin and depositional setting of the Kpwa–Atog Boga banded iron formations (BIFs), northwestern Congo craton, southern Cameroon. Ore Geol. Rev. 95, 620–638.

[35] Soh Tamehe, L., Chongtaoa, W., Ganno, S., Shaamu, J.S., Kouankap Nono, G.D., Nzenti, J.P., Lemdjoue, Y.B., Naing Htun, L., (2019). Geology of the Gouap iron deposit, Congo craton, southern Cameroon: Implications for iron ore exploration. Geology Reviews 107, pp. 1097–1128. https://doi.org/10.1016/j.oregeorev.2019.03.034.

[36] Ndema Mbongué, J.L., Luku, O.I., (2020). Geology and geochemistry of Messondo banded iron formation-hosted iron ore from the northwestern Congo Craton, southern Cameroon: implication for iron ore deposits. GSJ: Volume 8, Issue 2, February 2020.

[37] Nzenti, J.P, Barbey, P, Macaudiere, J. and Soba, D., (1988).Origin and evolution of the late Precambrian high-grade Yaounde gneisses (Cameroon). Prec Res. 38:91-109.

[38] Toteu, S.F., Van Schmus, W.R., Penaye, J., Nyobé, J.B., (1994). U-Pb and Sm-Nd evidence for Eburnean and Pan-African highgrade metamorphism in cratonic rocks of southern Cameroon, Precamb. Res. 67, 321-347.

[39] Tchameni, R., Mezger, K., Nsifa, N.E. and Pouclet, A. (2001). Crustal origin of early Proterozoic syenites in the Congo Craton (Ntem complex), South Cameroon. Lithos, 57, 23–42.

[40] Shang, C.K., Liégeois, J.P., Satir, M., Frisch, W. and Nsifa, E.N., (2010). Late Archaean high-K granite geochronology of the northern metacratonic margin of the Archaean Congo craton, southern Cameroon: Evidence for Pb-loss due to nonmetamorphic causes. Gondwana Res., 18, 337–355.

[41] Ndema Mbongué, J.L., Nzenti, J.P., Cheo, E.S., (2014). Origin and evolution of the formation of the Nyong serie in the Western Border of the Congo Craton. J Geosci Geom. 2(2):62-75.

[42] Ndema Mbongué, J.L., Sigué, C., Nzenti, J.P. and Cheo, E.S., (2019). Structural Characterization of Outcrop-Scale in Edea and Eseka Area: Evidence for a Complex Polyphase Deformation in the Paleoproterozoic Nyong Serie (Congo craton-South Cameroon). "IOSR Journal of Applied Geology and Geophysics (IOSR-JAGG) 7.5 (2019): 01-09.

[43] Nsifa, N.E., Tchameni, R., Nédélec, A., Siqueira, R., Pouclet, A., Bascou, J., (2013). Structure and petrology of Pan-African nepheline syenites from the South West Cameroon; Implications for their emplacement mode, petrogenesis and geodynamic significance. Journal of African Earth Sciences 87, 44–58.

[44] Maurizot, P., Abessolo, A., Feybesse, J.L., Johan, V., Lecomte, P., (1986). Etude et prospection minière du Sud-Ouest Cameroun. Synthese des travaux de 1978 à 1985. Rapport BRGM 85 CMR 066.

[45] Delhal, J. et Ledent, D., (1974). Musée Royal Afrique Centrale. Tervuren. Rapport. Annuel. pp. 71-76.

[46] Lasserre, M, and Soba, D., (1976). Age liberien des granodiorites et des gneiss a pyroxenes du Cameroun meridional. Bulletin du BRGM. 2:17–32

[47] Lerouge, C., Cocherie, A., Toteu, S.F., Penaye, J., Milési, J.P., Tchameni, R., Nsifa, E.N., Fanning, C.M., Doloule, E., (2006). Shrimps UPb zircon age evidence for Paleoproterozoic sedimentation and 2.05Ga syntectonic plutonism in the Nyong Group, SouthWestern Cameroon: consequences for the Eburnean-Transamazonian belt of NE Brazil and Central Africa. J Afr Earth Sci. 44, 413-427.

[48] Pouclet, A., Tcahameni, R., Mezger, K., Vidal, M., Nsifa, E.N., Shang, C. and Penaye, J., (2007). Archaean crustal accretion at the Northern border of Congo Craton (South Cameroon): The charnockite-TTG ling. Bull. Soc. Géol. France. 178: 331-342.

[49] Ebah Abeng, S.A.E., Ndjigui, P.D., Beyanu, A.A., Teutsong, T., Bilong. P., (2012). Geochemistry of pyroxenites, amphibolites and their weathered products in the Nyong unit, SW Cameroon (NW border of Congo Craton): Implications for Au-PGE exploration. Journal of Geochem. Expl, 114, 1-19.

[50] Actlabs (2019). Schedule of Services and Fees, Geochemistry – International.

[51] Siivola, J. and Schmid, R., (2007). List of Mineral Abbreviations. Recommen-dations by the IUGS Subcommission on the Systematics of Metamor-phic Rocks. Web version 01.02.2007; www.bgs.ac.uk.scmr/home.html.

[52] Taylor, S.R. and McLennan, S. M., (1985). The continental crust: its composition and evolution. Blackwell Publishing, Oxford, UK, 312.

[53] Bau, M., Dulski, P., (1996). Distribution of yttrium and rare-earth elements in the Penge and Kuruman Iron Formation, Transvaal Supergroup, South Africa. Precambrian Research 79, 37–55.

[54] Akagi, T. and Masuda, A., (1998). A simple thermodynamic interpretation of Ce anaomaly. Chemical Journal, 35(5); 301-314.

[55] Chombong, N.N., Suh, C.E., Lehmann, B., Vishiti, A., Ilouga, D.C., Shemang, E.M., Tantoh, B.S., Kedia, A.C., (2017). Host rock geochemistry, texture and chemical composition of magnetite in iron ore in the Neoarchaean Nyong unit in southern Cameroon. Appl. Earth Sci. http://dx.doi.org/10.1080/03717453.2017.1345507.

[56] Ndong B.F., Sobdjou K.C., Yannah M., Ntomba M.S., Nzenti J.P., Mvondo O.J., (2016). Origin and tectonic framework of the Ngovayang Iron Massifs, southern Cameroon. Sci. Res. 4, 11-20.

[57] James, H.L., (1966). Chemistry of the iron-rich sedimentary rocks, In: Fleischer M. (ed.), Data of Geochemistry', 6th edition, Paper 440-W, U.S. Govt. Printing Office, Washington D.C.

[58] James, H.L., (1992). Precambrian iron-formations: Nature, origin, and mineralogic evolution from sedimentation to metamorphism. In: Wolf, K.H., Chilingarian, G.V. (Eds.), Diagenesis III: Developments in Sedimentology, vol. 47. pp. 543–589.

[59] Herron, M.M., (1988). Geochemical classification of terrigenous sands and shales from core or log data. J. Sediment. Petrol. 58, 820–829.

[60] Basta, F.F., Maurice, A.E., Fontboté. L., Favarger, P.Y., (2011). Petrography and geochemistry of the banded iron formation (BIF) of Wadi Karim and Um Anab. Eastern Desert. Egypt: Implications for the origin of Neoproterozoic BIF. Precambrian Research 187. p. 277-292.

[61] Lan, T.G., Fan, H.R., Santosh, M., Hu, F.F., Yang, K.F., Liu, Y.S., (2014). U-Pb zircon chronology, geochemistry and isotopes of the Changyi banded iron formation in the eastern Shandong Province: constraints on BIF genesis and implications for Paleoproterozoic tectonic evolution of the North China Craton. Ore Geol. Rev. 56, 472–486.

[62] Mukherjee, S.K., (2008). Petrography, Age (U–Pb zircon), Geochemical and Isotopic Studies of the Sawawin Banded Iron-formation (BIF), Northwestern Saudi Arabia: Implications for Understanding Neoproterozoic Climate Change (Ph.D. thesis). University of Texas at Dallas, pp. 137.

[63] Dymek, R.F., Klein, C., (1988). Chemistry, petrology and origin of banded iron formation lithologies from 3800 Ma Isua supracrustal belt, West Greenland. Precambrian Res. 39, 247–302.

[64] Alexander, B.W., Bau, M., Andersson, P., Dulski, P., (2008). Continentally-derived solutes in shallow Archean seawater: rare earth element and Nd isotope evidence in iron formation from the 2.9 Ga Pongola Supergroup, South Africa. Geochim. Cosmochim. Acta 72, 378–394.

[65] Bau, M., Dulski, P., (1999). Comparing yttrium and rare earths in hydrothermal fluids from the Mid-Atlantic Ridge: implications for Y and REE behaviour during nearvent mixing and for the Y/Ho ratio of Proterozoic seawater. Chem. Geol. 155, 77–90.

[66] Michard, A., Michard, G., Stuben, D., Stoffers, P., Cheminee, J.-L., Binard, N., (1993). Submarine thermal springs associated with young volcanoes: the Teahitia vents, Society Islands Pacific Ocean. Geochim. Cosmochim. Acta 57, 4977–4986.

[67] Alibo, D.S., Nozaki, Y., (1999). Rare earth elements in seawater: particle association, shale normalization, and Ce oxidation. Geochimica et Cosmochimica Acta 63, 363–372.

[68] Bonatti, E., (1975). Metallogenesis at oceanic spreading centers. Annu. Rev. Earth and Planet. Sci. 3, 401–433.

[69] Ewers, W.E., Morris, R.C., (1981). Studies of the Dales George member of the Brockman Iron Formation, Western Australia. Econ. Geol. 76, 1929–1953.

[70] Arora, M., Govil, P.K., Charan, S.N., Uday Raj, B., Balaram, V., Manikyamba, C., Chatterjee, A.K., Naqvi, S.M., (1995). Geochemistry and origin of Archean banded iron–formation from the Bababudan Schist Belt, India. Econ. Geol. 90, 2040–2057.

[71] Maurice, A.E., (2000). Petrology and mineralization of Gebel Abu Marawat area, Eastern Desert, Egypt. M.Sc Thesis, Cairo University, 226p.

[72] Barrett, T.J., (1981). Chemistry and mineralogy of Jurassic bedded chert overlyingophiolites in the North Appenines, Italy. Chem. Geol. 34, 289–317.

[73] Marchig, V., Gundlach, H., Möller, P., Schley, F., (1982). Some geochemical indicatorsfor discrimination between diagenetic and hydrothermal metalliferoussediments. Mar. Geol. 50, 241–256.

[74] Sunder, P.V. Raju, (2009). Petrography and geochemical behavior of trace elements, REE and precious metal signatures of sulphidic banded iron formations from the Chikkasiddavanahalli area, Chitradurga schist belt, India. Journal of Asian Earth Science. 34 (5); 663-673.

[75] Rao, G.T. and Naqvi, S.M., (1995). Geochemistry depositional environment and tectonic setting of the Bif of late Archaean Chitradurga schist belt, India. Chem. Geol. 121: 217-243.

[76] Derry, L.A. and Jacobsen, S.B., (1990). The chemical evolution of Precambrian seawater: Evidence from REEs in banded iron formations. Geochimica et Cosmochimica Acta, 54, 2965-2977. doi:10.1016/0016-7037(90)90114-Z.

[77] Isley, A.E. and Abbott, D.H., (1999) Plume-related mafic volcanism and the deposition of banded iron formation. J. Geophys. Res., 104, 15461–15477.
[78] krapež, B., Barley, M.E., Pickard, A.L., (2003). Hydrothermal and resedimented origins of the precursor sediments to banded iron formation: sedimentological evidence from the Early Palaeoproterozoic Brockman Supersequence of Western Australia. Sedimentology 50, 979–1011.
[79] Holland, H.D., (1973). Ocean-possible source of iron in iron formations. Economic Geology, 68, 1169-1172. doi:10.2113/gsecongeo.68.7.1169.
[80] Nkoumbou, C. Fuh Calistus, Tchakounte Numbem, J.A., Belle Ekwe Lobe, Y.V., Nwagoum Keyamfe, C.S., (2017). Petrology and geochemistry of REE-rich Mafe´ banded iron formations (Bafia group, Cameroon). Comptes Rendus Geoscience. 349 (2017) 165–174.
[81] Klein, C., Beukes, N.J., (1989). Geochemistry and sedimentary of a facies transition from limestone to iron formation deposition in the Early Proterozoic Transvaal Supergroup, South Africa. Econ. Geol. 84, 1733–1774.
[82] Bau, M., Möller, P., (1993). Rare earth element systematics of the chemicallyprecipitated component in Early Precambrian iron-formations and theevolution of the terrestrial atmosphere–hydrosphere–lithosphere system.Geochim. Cosmochim. Acta 57, 2239–2249.
[83] Roser, B.P., Korsch, R.J., (1986). Determination of tectonic setting of sandstone–mudstone suites using SiO_2 content and K_2O/Na_2O ratio. J. Geol. 94, 635–650.
[84] Lepp, H. and Goldich, S.S., (1964). Origin of the Precambrian Iron-Formation. Economic Geology, 59, 1025-1060. https://doi.org/10.2113/gsecongeo.59.6.1025.
[85] Govett, G.J.S. (1966). Origin of Banded Iron-Formation. Geological Society of America Bulletin, 77, 1191-1212.
[86] Wright, J., Schrader, H. and Holser, W., (1987). Paleoredox variations in ancient oceans recorded by rare earth elements in fossil apatite. Geochim. Cosmochim. Acta 51, 631–644.
[87] Angerer, T., Hagemann, S.G. and Danyushevsky, L.V., (2012). Geochemical evolution of the banded iron formation-hosted high-grade iron ore system in the Koolyanobbing Greenstone Belt, Western Australia. Econ. Geol., 107, 599–644.
[88] Middleton, G.V., (1960). Chemical composition of sandstone. Geol. Soc. America Bull. 71; 1011-1026.
[89] Crook, K.W.A. (1974). Lithogeneses and geotectonics: the significance of compositional variation in flusch arenites (graywackes). Soc. Econ. Paleo. Min. Spec. Publ. 19; 304-310.
[90] Siever, R., (1979). Plate tectonics control on diagenesis. J. Geol., 88pp.
[91] Belevtsev, Y.N., Kravchenko, V.M., Kulik, D.A., Belevtsev, R.Y., Borisenko, V.G., Drozdovskaya, A.A., Epatko, Y.M., Zankevich, B.A., Kalinichenko, O.A., Koval, V.B., Korzhnev, M.N., Kusheyev, V.V., Lazurenko, V.I., Litvinskaya, M.A., Nikolayenko, V.I., Pirogov, B.I., Prozhogin, L.G., Pikovskiy, E.S., Samsonov, V.A., Skvortsov, V.V., Savchenko, L.T., Stebnovskaya, Y.M., Tereshchenko, S.I., Chaykin, S.I. and Yaroshchuk, M.A., (1991). Precambrian banded iron formations of the European part of the USSR. Genesis of iron-ores. Naukova Dumka Press, Kiev, Ukrainia (IGCP UNESCO Project, No 247 (in Russian).
[92] Morris, R.C., (2002). Genesis of high-grade hematite ore bodies of the Hamersley Province, Western Australia – A discussion. Econ. Geol., 97, 177–181.
[93] Adekoya, A.J., Okonkwo, C.T. and Adepoju, M.O. (2012). Geochemistry of Muro Banded Iron Formation, Central Nigeria. Int. J. Geosci., 3, 1074–1083.